Title (10 words, 15 words or less): PRAME Epitopes are T-Cell Immunovulnerabilities in *BRD4::NUTM1* Initiated NUT Carcinoma

Running Title (22 characters, <60 characters): *PRAME* in NUT Carcinoma

Authors: Jeffrey L. Jensen*††[1,2], Sara K. Peterson††[2,3], Shawn Yu[1,2], Tomoaki Kinjo[2,4], Brandon A. Price[5], Maria Sambade[2], Steven Vesko[2], Johnathan D. DeBetta[6], Julie K. Geyer[2,7], Kwangok P. Nickel[8], Randall J. Kimple[8,9], Rishi S. Kotecha[10,11,12], Ian J. Davis[2,13], Jeremy R. Wang[2,7], Christopher A. French[14], Brian Kuhlman[2,4], Alex Rubinsteyn[xx2,3], Jared Weiss[xx1,2], Benjamin G. Vincent[xx15,16]

†† = co-first authorship

xx = co-last authorship

* = corresponding author

Corresponding Author
Jeffrey Lee Jensen, MD/PhD
Division of Medical Oncology
Department of Medicine
University of North Carolina-Chapel Hill
101 Manning Drive
Chapel Hill, NC 27514
Jeffrey_Jensen@med.unc.edu

1: Division of Medical Oncology, Department of Medicine, The University of North Carolina at Chapel Hill, Chapel Hill, North Carolina
2: Lineberger Comprehensive Cancer Center, Chapel Hill, North Carolina
3: Department of Genetics, Curriculum in Bioinformatics and Computational Biology, The University of North Carolina at Chapel Hill, Chapel Hill, North Carolina
4: Department of Biochemistry and Biophysics, University of North Carolina at Chapel Hill, Chapel Hill, North Carolina
5: Tempus AI, Inc., Chicago Illinois
6: Department of Biochemistry and Molecular Biology, John Hopkins Bloomberg School of Public Health, Baltimore, Maryland
7: Department of Pathology and Laboratory Medicine, University of North Carolina at Chapel Hill, Chapel Hill, North Carolina
8: Department of Human Oncology, University of Wisconsin School of Medicine and Public Health, University of Wisconsin, Madison, WI
9: University of Wisconsin Carbone Cancer Center, University of Wisconsin School of Medicine and Public Health, University of Wisconsin, Madison, WI
10: Department of Clinical Haematology, Oncology, Blood and Marrow Transplantation, Perth Children's Hospital, Perth, Austrailia
11: Leukaemia Translational Research Laboratory, WA Kids Cancer Centre, The Kids Research Institute Austrailia, University of Western Austrailia, Perth, Austrailia
12: Curtin Medical School, Curtin University, Perth, Austrailia
13: Division of Hematology-Oncology, Department of Pediatrics, The University of North Carolina at Chapel Hill, Chapel Hill, North Carolina
14: Department of Pathology, Brigham and Women's Hospital, Harvard Medical School, Boston, Massachusetts
15: Division of Hematology, Department of Medicine, The University of North Carolina at Chapel Hill, Chapel Hill, North Carolina
16: Department of Microbiology and Immunology, The University of North Carolina at Chapel Hill, Chapel Hill, North Carolina

The authors declare no potential conflicts of interest.

Abstract (Words=148, Word Limit=150):

NUT carcinoma ("NC") is a rare but highly lethal solid tumor without an effective standard of care. NC is caused by bromodomain-containing *NUTM1* fusion genes, most commonly *BRD4::NUTM1*. BRD4::NUTM1 recruits p300 to acetylate H3K27 forming "megadomains" with the overexpression of encapsulated oncogenes, most notably *MYC*. Akin to *MYC*, we hypothesized that transcriptional dysregulation caused by BRD4::NUTM1 would lead to the generation of cancer specific antigens that could be therapeutically actionable. Integrating genomics, immunopeptidomics, and computational biology approaches, we identified *PRAME* as the predominantly transcribed and HLA Class I-presented cancer/testis antigen in NC. Further, we show that a PRAME epitope-specific T-cell receptor ("TCR") x CD3 activator bispecific molecule modeled after brenetafusp has potent T-cell mediated activity against PRAME+ NC. Our results show that PRAME is often highly expressed in NC due to BRD4::NUTM1, and that BRD4::NUTM1 induced PRAME antigens are promising TCR targets for forthcoming clinical trials in NC.

Statement of Significance (49 words, 50 word limit):

NC is one of the most aggressive solid tumors to afflict humans and is refractory to chemotherapy, T-cell checkpoint blockade, and targeted therapies. We show PRAME epitopes are promising targets for TCR-based therapeutics like brenetafusp in NC, adding to growing momentum for addressing challenging fusion malignancies with TCR therapeutics.

Introduction (Words=635):

NC is a rare but underdiagnosed and devastating malignancy defined by ectopic expression of the Nuclear Protein in Testis gene ("*NUT*" or "*NUTM1*"), most commonly through an in-frame translocation to the bromodomain-containing *BRD4* with formation of the *BRD4::NUTM1* fusion gene (75% of cases) [1]. BRD4::NUTM1 is a potent oncoprotein that initiates NC by binding to acetylated H3K27 ("H3K27ac"), recruiting p300 and catalyzing the hyperacetylation of adjacent histones resulting in extended hyperacetylated domains ("megadomains") with the corresponding overexpression of oncogenes, including *MYC* and *SOX2* [2, 3]. NC was formerly labeled as NUT Midline Carcinoma owing to a predilection for afflicting midline structures and is now known to occur most commonly in the lungs and sinonasal passages [4]. NC is not associated with smoking or any known exposures and afflicts individuals of all ages including infants, children, and young adults [5-7]. Clinical outcomes in adults are dismal with median survival after diagnosis of 6.7 months and similar outcomes in children [4, 8]. Treatment for localized disease is focused on aggressive attempts at local control with wide local resection and adjuvant radiation and/or chemotherapy, but even among NC patients treated with surgery first outcomes are poor. In one cohort, surgery first patients experienced a median survival time of 415 days post-diagnosis with no patient surviving for more than 3 years post diagnosis [4, 9].

Therapeutics research to date has focused on blocking the binding of BRD4 to H3K27ac using bromodomain inhibitors, but in phase I/II clinical trials bromodomain inhibitors have yielded progression free survival times of only 1-2 months [10-13]. At the time of this

writing, all clinical trials testing new therapeutics for NC patients in the United States are testing bromodomain inhibitors (NCT05019716, NCT05372640, and NCT05488548). NC tumors are PD-L1 low, tumor mutational burden low, and immune “cold” tumors that are also highly refractory to cytotoxic chemotherapy and T-cell checkpoint blockade [4]. New treatment modalities are desperately needed.

Interest in treating challenging solid tumors with HLA-restricted T-cell receptor (“TCR”)-based therapies is growing. The first phase III clinical trial of a TCR x CD3 activator bispecific (“ImmTAC”) showed overall survival benefit in the frontline setting for HLA A02+ uveal melanoma targeting the gp100 peptide [14]. Recently, the SPEARHEAD-1 trial showed durable responses in patients with heavily pre-treated synovial sarcoma or myxoid round cell liposarcoma with afamitresgene autoleucel: a TCR T-cell therapy expressing a TCR targeting an HLA-A02 bound epitope from the cancer/testis gene *MAGEA4* [15]. This resulted in the first TCR T-cell product approval for afamitresgene autoleucel and was quickly followed up by the IGNYTE-ESO trial which similarly showed durable responses in the same disease types with letetresgene autoleucel: another TCR T-cell product targeting epitopes from the cancer/testis gene *NY-ESO-1* (HLA A*02:01, A*02:05, or A*02:06) [16].

Like NC, both synovial sarcoma and myxoid/round cell liposarcoma are uncommon fusion protein-driven malignancies. For each of these sarcomas, >90% of cases harbor the pathognomonic t(X;18) or t(12;16)(q13;p11), respectively [17, 18]. Whereas MAGEA4 and NY-ESO-1 antigens are common in these sarcomas, the antigenic landscape of NC

and the susceptibility of NC to T-cell mediated therapeutics are unknown. We hypothesized that if BRD4::NUTM1 causes dysregulated gene transcription through reliable epigenetic changes, then BRD4::NUTM1 could also upregulate genes encoding cancer specific antigens that would serve as actionable TCR targets. Here we show that BRD4::NUTM1 causes transcription of the cancer/testis gene *PRAME*, and that *PRAME* is the predominant cancer/testis gene expressed within a clinical patient cohort of *NUTM1* fusion genes and especially in patients with canonical NC fusions (*BRD4::NUTM1*, *BRD3::NUTM1*, *NSD3::NUTM1*) [19]. We also show that NC cells present PRAME epitopes with HLA Class I and are susceptible to T-cell mediated killing enhanced by an affinity-matured PRAME epitope TCR x CD3 activating bispecific molecule. Our work identifies PRAME as a promising target for cancer vaccines, TCR-based therapies, and TCR-mimetics in NC phase I/II clinical trials.

Results (Word Count = 1,564)

NC cells have preserved expression of genes involved in antigen presentation and are susceptible to allogeneic T-cell cytotoxicity

To address whether T-cell-based, antigen-directed immunotherapy would be applicable in NC, we first sought to assess the antigen presentation capacity of NC cells and their susceptibility to T-cell killing. We performed short read RNA sequencing on five *BRD4::NUTM1* NC cell lines and a *BRD3::NUTM1* patient derived xenograft ("PDX"). We then obtained HLA haplotypes and compared expression of HLA alleles and antigen presentation genes to normal lung tissue. We found that samples other than the JCM1 cell line were HLA A02:01+ (**Figure 1A**), and we found similar HLA Class I pathway gene expression in NC and healthy lung but markedly higher HLA Class II allele expressions in healthy lung (**Figure 1B**). This is consistent with the rich inundation of lungs with professional antigen presenting cells and their elevated levels of HLA Class II gene expression. To evaluate whether NC cell lines can be killed by activated T-cells, we co-cultured NC cells with allogeneic pan T-cells from human peripheral blood and stimulated the T-cells them with ImmunoCult CD3/CD28 T-cell activator (Stemcell Technologies) and/or atezolizumab (R&D systems). We found similar T-cell dependent tumor cell killing between NC and two non-small cell lung cancer ("NSCLC") lines that was enhanced by CD3/CD28 activation and not dependent on atezolizumab (**Figure 1C**). We concluded that congruous with outcomes in patients, T-cell activation with PD1/PDL1 inhibition does not provoke a cytotoxic response against NC cells, but that CD3-activating mechanisms may.

RNA sequencing and computational predictions suggest PRAME and NUTM1 are sources of HLA Class I peptide ligands in NC

We proceeded to identify promising antigens for TCR targeting by applying the LENS computational workflow to RNA sequencing of the NC cell lines and the PDX (**Figure 2**). LENS is an open-source method that predicts tumor-specific and tumor-associated antigens from genomic data [20]. LENS predicted HLA Class I ligand binding in several CTAs but across multiple samples, only PRAME and NUTM1 reliably had predicted epitopes. Interestingly, LENS predicted the translationally relevant $PRAME_{425-433}$ SLLQHLIGL epitope in every sample except for TC-797 in which PRAME was transcriptionally silent [21, 22]. In screening cancer/testis genes using our manually curated list of CTAs (**Supplementary Methods Table 3**), out of 164 different cancer/testis genes only *PRAME* was consistently expressed across the tested samples. We concluded that in cell lines and the PDX, PRAME and NUTM1 are the most promising sources of cancer specific antigens.

To determine if this finding was reflected in patient samples, we searched the de-identified Tempus multimodal database for patients with detected *NUTM1* fusion genes (identified via Tempus xT [solid-tumor DNA] [23], Tempus xR [solid-tumor RNA] [24], or Tempus xF [circulating tumor DNA] assays) [25]. Research filters below clinical reporting were applied to obtain patients with evidence of a *NUTM1* fusion, defined as containing at least 10 total supporting reads from DNA or at least 5 total supporting reads from RNA. Subject to these thresholds, 165 patients had evidence of *NUTM1* fusions, with a total of 33 distinct fusion partners (**Table 1**). Consistent with their role as canonical NC fusion partners, *BRD4::NUTM1, NSD3::NUTM1, BRD3::NUTM1* accounted for the majority of

cases (35.8%, 17.6%, and 10.9% respectively) with the remaining samples harboring one of the 30 other fusion partners (**Supplementary Figure 2A).** As expected, *BRD4::NUTM1*, *BRD3::NUTM1*, and *NSD3::NUTM1* fusions primarily occurred in the lung and head/neck primary sites – typical locations for NC [9]. Analysis of gene expression from 162 of the patients with available RNA data revealed that out of 157 CTA genes covered in the Tempux xR assay, *PRAME* was identified as having the highest average expression after *NUTM1* (**Figure 3A**). We observed a bimodal distribution of *PRAME* expression in comparison to *NUTM1* across the cohort, designating *PRAME*^{high} and *PRAME*^{low} groups using a threshold of 3.1 $\log_2$(TPM+1) (**Figure 3B**). We found the *BRD4::NUTM1* group to be significantly enriched in PRAME^{high} samples (fisher exact, $p<0.001$) with *BRD3::NUTM1* and *NSD3::NUTM1* also having more PRAME^{high} samples than PRAME^{low} (**Figure 3C**). Of the remaining non-canonical fusion partners, 14 partners had at least one instance of PRAME^{high} with 3 fusion partners having more than one: *MGA::NUTM1*, *SLC12A6::NUTM1*, and *CIC::NUTM1* (**Supplementary Figure 2B**). Notably, only 1 of 13 *YAP1::NUTM1* samples was classified as PRAME^{high}. Using the *PRAME*^{high} and *PRAME*^{low} groups, we identified several primary sites with the highest percentage of *PRAME*^{high} samples (**Figure 3D**). These sites included multiple sinus regions, unspecified peripheral nervous system (PNS), thymus, trachea, liver, and vulva; most lung and head, face, or neck primary sites demonstrated high *PRAME* expression. To assess for protein level PRAME expression in NC patient samples, we also stained a previously described NC tissue microarray for PRAME and found PRAME staining in 43/77 (56%) of samples (**Figure 3E**) [26].

BRD4::NUTM1 and MYC drive PRAME expression and HLA Class I epitope presentation in NC

Given that *PRAME* transcripts are high in NC and that *PRAME* expression is regulated by epigenetic changes including H3K27 acetylation in non-malignant human physiology [27], we hypothesized that BRD4::NUTM1 might be causing increased transcription of *PRAME*. To test this hypothesis, we transduced HEK 293T cells with tet-on *BRD4::NUTM1* or *GFP* lentiviral particles and observed an increase in PRAME protein levels with *BRD4::NUTM1* expression but not with GFP (**Figure 4A**). We then used siRNAs targeting *NUTM1* to knockdown BRD4::NUTM1 in the five NC cell lines and immunoblotted for PRAME (**Figure 4B top**). We found that in all cell lines except for the *PRAME* negative TC-797 cell line, BRD4::NUTM1 loss was accompanied by a decrease in PRAME protein levels. The decrease in PRAME with BRD4::NUTM1 knockdown was marginal in 14169 compared to other NC cell lines, so we performed a western blot time course in 14169 cells which revealed a greater effect on PRAME levels at a later timepoint, 4 days instead of 3 days, after *NUTM1* siRNA transfection (**Figure 4B bottom**). To test whether BRD4::NUTM1 was activating *PRAME* expression through MYC, we also silenced MYC in the NC cell lines and found that in 10-15, PER-403, and JCM1 marginal decreases in PRAME were associated with MYC loss suggesting that both MYC and BRD4::NUTM1 maintain the high PRAME levels observed in BRD4::NUTM1 patient samples (**Figure 4C**).

We hypothesized that since cytosolic PRAME levels are high in NC, that HLA-bound PRAME epitopes would be detectable using untargeted mass spectrometry/immunopeptidomics. Untargeted mass spectrometry was performed with

the five cell lines and with the PDX to identify and characterize NUTM1, PRAME, and other CTA epitopes being presented by HLA Class I molecules and to guide therapeutic TCR selection in combination with our computational predictions. We identified a total of 33,644 unique peptides, 159 of which were shared by all samples **(Supplementary Figure 3**). Focusing on the presented CTAs, we identified 14 unique peptides from 6 proteins out of all CTAs with detection in at least 1 sample. Of these 14 peptides, 9 corresponded to PRAME and 1 corresponded to NUTM1 (**Figure 4E**). The remaining four CTA peptides corresponded to KKCL1, MAGA1, CTGE2, and ACTL8. As expected, the *PRAME* negative TC-797 revealed no PRAME epitopes. The well described $PRAME_{425}$ SLLQHLIGL epitope was detected in the HLA A02+ PER-403 and PDX samples [28-30]. To detect fusion junctional peptides, long read RNA sequencing was performed and used to generate consensus fusion sequences (**Supplementary Figure 4**). The reference human proteome was augmented with these fusion sequences for peptide mapping, but no junctional fusion peptides were detected. Based on the increased prevalence of PRAME epitopes in our samples relative to NUTM1 and based on the availability of existing PRAME therapeutics for testing, we hypothesized PRAME epitopes are more likely to be imminently actionable than NUTM1 epitopes in NC.

Transcriptionally PRAME+ but not PRAME- NC cells are susceptible to killing mediated by a PRAME epitope TCR x CD3 activator bispecific molecule

Whether NC is susceptible to TCR-mediated therapeutics like TCR bispecifics or TCR T-cell therapies is unknown. To explore this issue and to evaluate the translational relevance of PRAME cancer specific antigens, we created an HLA-A02 $PRAME_{425}$

SLLQHLIGL specific, affinity matured TCR x CD3 Fab activating bispecific molecule modeled after brenetafusp (**Figure 5A**). We used SLLQHLIGL peptide pulsing and TAP deficient T2 cells in co-culture with allogeneic T-cells to demonstrate enhancement of bispecific-mediated cytotoxicity with peptide pulse. TAP deficient T2 cells have empty HLA molecules on the cell surface and are loaded by incubating the cells in the presence of peptide ligands that will bind HLA. Killing of peptide-pulsed T2 cells thus demonstrated the specificity of the bispecific molecule for the SLLQHLIGL epitope (**Figure 5B**). We then titrated the concentration of the bispecific in the co-cultures of PRAME+ NSCLC cell lines in the presence of allogeneic T-cells and found a dose-dependent effect (**Figure 5C**). The *PRAME* negative TC-797 and the *PRAME* positive 10-15 and 14169 NC cell lines were tested alongside a haplo-incompatible NSCLC cell line (H460, HLA A*24:02, *68:01 [31]) for T-cell mediated cytotoxicity in co-culture experiments using 10^{-8} M of bispecific. We observed no cytotoxic effect of the bispecific in TC-797 or H460 at either of the tested effector: target ratios even with a SLLQHLIGL peptide pulse but we did observe potent cytotoxicity that was enhanced by a higher effector:target ratio and by peptide pulsing in both PRAME positive NC cell lines (**Figure 5D**). Interestingly, the SLLQHLIGL epitope was predicted by LENS in 10-15 and 14169 but not detected using untargeted mass spectrometry likely due to the limited sensitivity of immunopeptidomics [32-34].

Discussion (Words = 770)

Recent advances in antigen-directed immunotherapy have resulted in a new generation of “targeted immunotherapies” that leverage cell surface protein or TCR/peptide/HLA binding interactions for tumor targeting and specificity. Approved agents in solid tumors target either HLA-presented peptide epitopes such as gp100 in uveal melanoma, MAGEA4/NY-ESO-1 epitopes in synovial sarcoma/myxoid round cell liposarcoma [14, 15], or surface targets such as DLL3 in small cell lung cancer. To identify promising targeted immunotherapies for NC, a highly lethal and treatment-refractory malignancy, we performed RNA sequencing on a selection of NC samples and applied the results to the antigen prediction software LENS which predicted PRAME as a plentiful source of cancer-specific antigens in NC and a dearth of other CTAs [20]. We found that *PRAME* was highly expressed in cell lines and the PDX model, consistent with observations in a large cohort (N = 171) of *NUTM1* fusion patient samples and especially among canonical *NUTM1* fusion patient samples.

Using genetic approaches, we further showed that elevated PRAME levels in *BRD4::NUTM1* NC are enhanced or at least maintained by BRD4::NUTM1 and MYC. By applying immunopeptidomics to our panel of NC samples we also confirmed 9 PRAME epitopes, including the actionable SLLQHLIGL that is targeted by the ImmTAC brenetafusp. NUTM1 epitopes were nearly absent from our immunopeptidomics results, likely due to immunoselection for non-antigenic fusion proteins, limitations of detection by shotgun immunopeptidomics, and/or strong nuclear localization of NUTM1 fusion proteins [13]. PRAME epitopes are appealing candidates to be mechanistic antigens in NC:

antigens that are reliably present across NC patients because they arise as a direct result of the initiating genetic lesion in NC. We created a $PRAME_{425}$ SLLQHLIGL TCR x CD3 Fab bispecific molecule that then showed potent, T-cell-mediated cytotoxicity against *PRAME*+ NC cells but not *PRAME*- NC cells. In total we showed here that the most common oncogene initiating NC, *BRD4::NUTM1*, enhances *PRAME* transcription, that *PRAME* is a prevalent and highly expressed cancer/testis gene in *BRD4::NUTM1, NSD3::NUTM1* and *BRD3::NUTM1* NC, and that PRAME epitopes are actionable targets for TCR therapeutics in NC.

Our work adds NC to the growing cadre of malignancies for which there is immense interest in targeting PRAME. Specifically, PRAME prevalence is high in genetically heterogeneous cancers including melanoma, acute myeloid leukemia, NSCLC, ovarian cancer, and others [35]. In healthy human physiology, *PRAME* is turned on at the earliest stages of spermatogenesis and is silenced by histone modifications upstream of the translation initiation site [27]. In malignancies, PRAME expression has been associated with worse clinical outcomes, DNA double strand breaks, aneuploidy, and genetic instability [27, 36-38]. Oncogenic selection pressures in NC likely favor overriding the natural protections against ectopic PRAME production via BRD4::NUTM1-p300 acetylation of H3K27 [2, 26, 39]. EZH2 is active in NC and promotes inhibitory trimethylation of H3K27 which is mutually exclusive with H3K27ac domains in NC [26]. Thus, H3K27 trimethylation is a plausible mechanism by which TC-797 and other *BRD4::NUTM1* patient samples could restrict *PRAME* expression. Whole genome long-read DNA sequencing failed to identify a genetic cause for the absence of PRAME

expression (data not shown). Ultimately, further assays of histone states, such as ChIP-Seq or CUT&RUN, could explore this possibility. The mechanisms promoting transcription of *PRAME* are likely conserved between BRD4::NUTM1, BRD3::NUTM1, and NSD3::NUTM1 because BRD4 and BRD3 are highly homologous (>80%) and because NSD3::NUTM1 recruits BRD4, thus forming a protein complex with the same constituents as BRD4::NUTM1 [19, 40].

A blossoming array of PRAME targeting TCR therapeutics including TCR T-cell therapies, endogenous T-cell therapy, TCR bispecifics/ImmTACs, tumor vaccines, and/or immunoglobulins specific for HLA-bound PRAME epitopes ("TCR mimetics") may prove clinically effective in this challenging cancer. These agents include brenetafusp, the second ImmTAC in clinical testing, which has completed Phase I trials in platinum-resistant ovarian cancer and cutaneous melanoma [21, 22]. A PRAME-specific TCR is included in the presently recruiting trial NCT05973487: a personalized TCR T-cell trial for patients with locally advanced or metastatic solid tumors. An RNA-loaded dendritic cell vaccine using *PRAME* has completed phase I testing for allogeneic stem cell transplant-ineligible acute myeloid leukemia and other PRAME vaccines are in development [41, 42]. Pr20, a PRAME-specific TCR mimetic has been developed and showed activity against human leukemias in xenografts [43].

This growing set of PRAME therapeutics may have greater efficacy in NC than in NSCLC or other common malignancies without unifying genetic etiologies because of the mechanistic link between the central genetic rearrangements in NC and *PRAME*

expression. Clinical trials testing PRAME therapeutics like brenetafusp, Pr20, PRAME vaccines, or PRAME TCR T-cells in NC are a logical next step especially given the moral imperative of discovering efficacious treatments for this rare, orphan disease patient population.

Methods (Word Count = 1,843):

Cell Culture

TC-797, 10-15, 14169, PER-403, and JCM1 cell lines were maintained in Dulbecco's Modified Eagle Medium with 10% fetal bovine serum and penicillin/streptomycin. All cell lines and luciferase-expressing derivatives were generously provided by Dr. Christopher French. The patient-derived xenograft was provided by Dr. Randy Kimple and propagated in the flanks of NSG mice with Matrigel. Prior to genomic analysis, human cells were purified from the xenograft using a tumor dissociation kit (Catalog 130-095-929, Miltenyi Biotec) and a mouse cell depletion kit (Catalog 130-104-694, Miltenyi Biotec).

Reagents

RNA was isolated using RNEasy columns (Qiagen). All western blots were performed using PVDF membrane for transfer and blocking in 5% dried milk in T-BST. Primary antibodies and secondary antibodies are described in Supplementary Methods Table 1. siRNA transfections were performed per manufacturer specifications using Lipofectamine RNAiMAX (Thermo Fisher Scientific) and 10 μM pools of four siRNAs synthesized by IDT with [dT][dT] overhang, desalted purification, and no 3' modifications. siRNA sequences are provided in Supplementary Methods Table 2. MYC siRNAs and negative target control siRNAs were purchased commercially (Dharmacon ON-TARGETplus siRNA Gene ID 4609 and ON-TARGETplus Non-targeting Pool). Tet-on, blasticidin selection lentiviral pInducer20 vectors containing *BRD4::NUTM1* or *GFP* were generously provided by Dr. Christopher French. VSV-G pseudotyped lentiviral particles were generated in HEK 293T cells and purified by filtration and then used to transduce target 293T without

centrifugation or transduction additives (i.e., polybrene). Tissue microarray immunohistochemistry was done by BWH Dana-Farber-Harvard Medical School Specialized Histopathology Services-Longwood (SHL) Core facility using αPRAME (Biocare Medical, ACI3252B 1:100).

Computational Immunopeptidome Predictions

Samples were processed for tumor antigen prediction using Landscape of Effective Neoantigen Software ("LENS") v1.2-dev. Sample-level FASTQs were trimmed and filtered for quality using FASTP 0.23.1. The resulting FASTQ pairs were aligned to a modified hg38 reference genome (excluding the Epstein-Barr Virus (EBV) contig) using STAR 2.7.0f with parameters *--quantMode TranscriptomeSAM --outSAMtype BAM SortedByCoordinate --twopassMode Basic --outSAMunmappedWithin*. Transcript-level quantifications were generated using Salmon 1.1.0 with a GENCODE v37 GTF, augmented with human retroviral-like sequences from gEVE. Cancer testis antigens (CTAs) were defined using a manually curated list of genes with testis and placenta-specific expression (Supplementary Methods Table 3). The initial list of CTAs was pulled from CTDatabase (http://www.cta.lncc.br/) and was manually filtered using by Human Protein Atlas (allowing only testis and placenta protein staining). Where RNA only information was available, a literature search was conducted to determine tissue specific expression. Notably, NUTM1 was not on the list and was manually added at the authors' discretion.

Splice variants were detected using NeoSplice. Expressed viruses were detecting using the VirDetect workflow. HLA typing for class I alleles was performed using seq2HLA 2.2

with the trimmed RNA FASTQs. We processed protein sequences from CTAs in the 95th expression percentile for downstream peptide prediction. Gene fusions were predicted using STARfusion 1.10.1 with recommended parameters and trimmed RNA FASTQs. Finally, relevant protein sequences derived from CTAs, fusion, splice variants, viruses, and ERVs were filtered for potential peptides of interest using NetMHCpan 4.1b.

Bispecific Protein Production

Coding sequences for PRAME soluble TCR specific for the HLA-A*02:01-restricted SLLQHLIGL epitope were derived from sequences previously described elsewhere for the PRAME Vα and Vβ domains and from the Protein Data Bank ID 6U07 crystal structure for the computationally thermostabilized Cα and Cβ domains [44, 45]. Chimeric SP-34 anti-CD3 heavy and light chain sequences were published previously [46]. One primary fusion construct and two auxiliary constructs were generated as clonal genes in mammalian expression vector plasmids (Twist Bioscience). The primary fusion constructs consisted of the SP-34 anti-CD3 heavy chain, a $(Gly_4Ser)_4$ linker, PRAME TCR Vα/Cα, and an 8xHis-Tag. The first auxiliary coding sequence encoded for SP-34 anti-CD3 light chain; the second for PRAME TCR Vβ/Cβ. Amino acid sequences are provided in Supplemental Methods Table 4.

All three plasmid constructs were co-transfected for transient expression in Expi293F cells cultured with Expi293™ Expression Medium (Thermo Fisher Scientific, Catalog #A1435101) at 50 mL scale using ExpiFectamine™ 293 Transfection Kit (Thermo Fisher Scientific, Catalog #A14525), similarly to previously described with the following modifications [47]. Plasmids for primary fusion construct, first auxiliary construct, and

second auxiliary construct were mixed in a 3:1:1 mass ratio, totaling 1 μg plasmid mixture per milliliter of cell culture. At 18 hours after transfection, enhancer 1 (300 μL at 50 mL scale) and enhancer 2 (3 mL at 50 mL scale) and 6 mL of 3.5% (w/v) Hyclone Cell Boost 1 (GE Healthcare) were added to the cells. Cell culture supernatant was harvested at 96 hours after transfection by pelleting cells at 3428 relative centrifugal force (RCF) at 4°C for 15 min and further clarified using a 0.22 μm polyvinylidene difluoride membrane filter (Millipore). Assembled PRAME bispecific constructs were affinity purified by batch-binding clarified medium with pre-equilibrated penta-Ni resin (Marvelgent) for 1 hour at 4° C and then transferred into a column to collect the resin. A three-step wash was performed by gravity at room temperature (RT) to eliminate protein contaminants. The first wash was performed with 6 CV (column volume) of high-salt Tris buffer [50 mM Tris (pH 8.0) and 1 M sodium chloride with 10 mM imidazole]; the second was performed with 2 CV wash with 1× PBS (pH 7.4) with 20 mM imidazole; and the third was performed with 2 CV wash with 1× PBS (pH 7.4) with 40 mM imidazole. Bound proteins were eluted in one step using 5 CV of 1× PBS (pH 7.4) and 500 mM imidazole to collect the protein and then sequential concentration at 4°C using a 30K MWCO Amicon-4 followed by an Amicon-0.5 centrifugal filter at maximum allowed RCF for each filter, serially exchanged into 1× PBS (pH 7.4) to ensure at least 1:1000 dilution of imidazole. Purity was assessed by SDS-polyacrylamide gel electrophoresis (SDS-PAGE) under non-reducing conditions.

Cytotoxicity Assays

Human CMV negative whole blood was obtained from Gulf Coast Regional Blood Center. Peripheral blood monocytes were isolated using Ammonium-Chloride-Potassium Lysing

Buffer (ThermoFisher) and Density Gradient Medium (Stemcell Technologies) per manufacturer specifications. T-cells were isolated using a negative selection, magnetic bead kit (EasySep Human T Cell Isolation Kit, Stemcell Technologies) and then incubated with RPMI and 10% fetal bovine serum for 5 days in an αCD3 coated (5 μg/mL, BD Biosciences) tissue culture treated flask with carrier-free IL-2 (2 ng/mL, R&D Systems) and αCD28 (2.5 μg/mL, BD Biosciences) prior to co-culture. For some assays, peripheral blood CD3+ cells were purchased from BioTrend USA (supplier CGT Global) and used in lieu of in-house isolated T-cells. Expanded human T-cells were co-cultured in RPMI media with 10% FBS and white 96 well plates and then luminescence output was either read using CellTiter-Glo 2.0 reagent (Promega) for luciferase-free cell lines or by adding *in vivo*-grade luciferin (Promega) to a final concentration of 250 μg/mL for luciferin-expressing cell lines. Plates were read using a BioTek Synergy 2 Plate Reader. Peptide pulses were performed using 1 μg/mL of SLLQHLIGL peptide, synthesized by the UNC High-Throughput Peptide Synthesis and Array Facility, over at least three hours.

RNA Sequencing

Library preparation was performed using Illumina's Stranded mRNA Prep Ligation kit, starting with 125 ng of total RNA. This method uses oligo(dT) magnetic beads to capture mRNAs with polyA tails. The average fragment length for these libraries was between 300-400 bp. Paired-end sequencing was performed using the NovaSeq 6000 version 1.5 (2X100), obtaining at least 45M reads per sample. Bulk RNA-seq samples were processed using selected components of the nf-core RNA-seq pipeline (v3.14), an open-source workflow managed with Nextflow. Reads were demultiplexed, and quality was

assessed using FastQC, with results summarized in MultiQC. Adapter trimming was performed with cutadapt, ribosomal RNA was removed with SortMeRNA, followed by alignment to the GRCh38 reference genome using STAR. Transcript-level quantification was conducted with Salmon. Counts were then summarized to the gene level and normalized to transcripts per million (TPM) to generate a gene x sample matrix. All downstream visualization and analysis were performed in R (v4.4). All scripts used for this project are publicly available on GitHub (https://github.com/pirl-unc/PRAME_in_NUT_Carcinoma). Healthy lung tissue RNA sequencing data is publicly available [48]. FASTQ files were downloaded from Array Express Archive (www.ebi.ac.uk/arrayexpress/) under the accession number: E-MTAB-1733. Metadata was used to subset only 'lung' samples from all other tissue samples.

Immunopeptidomics

Snap frozen cell pellets were submitted to Biognosys for MHC Class I immunopeptidome profiling. These samples and a processing quality control sample (human JY cells) were lysed using Biognosys' Lysis Buffer for 1 hour at 4° C. After removal of cell debris, the lysates were incubated with beads coupled antibodies (clone W6/32) to capture HLA class I complexes with associated peptides. After immunoprecipitation, bound protein complexes were washed and peptides eluted using Biognosys' optimized immunopeptidomics protocol. Clean up for mass spectrometry was carried out using an Oasis HLB µElution Plate (30 µm) according to the manufacturer's instructions. Immunopeptides were dried down using a SpeedVac system and resuspended in 10 ul of 1% acetonitrile and 0.1% formic acid in water. Samples were pooled and fractionated

into 5 fractions using high pH reversed phase fractionation (HPRP) for spectral library generation.

For DDA LC-MS/MS measurements of fractionated samples, 8 µl of immunopeptides per sample were injected to a Biognosys in-house packed reversed-phase column on a Thermo Scientific NeoVanquish UHPLC nano liquid chromatography system connected to a Thermo Scientific Orbitrap Exploris 480 mass spectrometer equipped with a Nanospray Flex ion source and a FAIMS Pro ion mobility device (Thermo Scientific). LC solvents were A: water with 0.1% FA, B: 80% acetonitrile. The nonlinear LC gradient was 1 - 40% solvent B in 120 minutes followed by a column washing step in 90% B for 11 minutes, and a final equilibration step of 1% B for 5 minutes at 64° C with a flow rate set to 250 nl /min. MS1 precursor scans were acquired between 330-1250 m/z at 120,000 resolution with data dependent MS2 scans at 60,000 resolution. MS2 scans were acquired in cycle time of 1.6 s and 1.4 s per applied FAIMS compensation voltage. Only precursors with charge state 1-5 were isolated for dependent MS2 scans.

For DIA LC-MS/MS measurements of study samples, 8 µl of immunopeptides per sample were injected to a Biognosys in house packed reversed phase column on a Thermo Scientific NeoVanquish UHPLC nano liquid chromatography system connected to a Thermo Scientific Orbitrap Exploris 480 mass spectrometer equipped with a Nanospray Flex ion source and a FAIMS Pro ion mobility device (Thermo Scientific). The system was used in trap and elute configuration using a 300 µm x 5 mm PepMap Neo C 18 Trap 3 PK cartridge pre column (Thermo Scientific 174502). LC solvents were A: water with 0.1% FA, B: 80% acetonitrile, 0.1% FA in water. The nonlinear LC gradient was 1-40% solvent B in 120 minutes followed by a column washing step in 90% B for 11 minutes, and a final

equilibration step of 1% B for 5 minutes at 64° C with a flow rate set to 250 nl /min. The FAIMS DIA method consisted of one full range MS1 scan and 20 DIA segments as adopted from Bruderer et al [49] and Tognetti et al [50].

Acknowledgments:

JLJ was supported by a Conquer Cancer Young Investigator Award, paid for by the New Rhein Foundation. Any opinions, findings, and conclusions expressed in this material are those of the author(s) and do not necessarily reflect those of the American Society of Clinical Oncology®, Conquer Cancer®, or the New Rhein Foundation. JLJ was supported additionally by a Lung Cancer Initiative Fellowship Award, the UNC Department of Medicine Core Facilities CFAC Award, as well as the IM-TAG T32. RJK was supported by P50CA278595, R37 CA255330, and P30 CA014520. This work was also supported by The Max Vincze Foundation (AR and BGV), The Victor Family Foundation (AR and BGV), philanthropic support from the Ben Brown Family (JW), and the NIH grant R35GM131923. IJD is supported by the V Foundation for Cancer Research and the NIH (R01-CA276663). We would also like to acknowledge the work and contributions from multiple core facilities at UNC including the Immune Monitoring and Genomics Facility (IMGF), the High Throughput Sequencing Facility (HTSF), and the lentiviral/shRNA core facility.

References

1. Eagen KP, French CA. Supercharging BRD4 with NUT in carcinoma. Oncogene. 2021;40(8):1396-408.
2. Alekseyenko AA, Walsh EM, Wang X, Grayson AR, Hsi PT, Kharchenko PV, et al. The oncogenic BRD4-NUT chromatin regulator drives aberrant transcription within large topological domains. Genes & Development. 2015;29(14):1507-23.
3. Wang R, Liu W, Helfer CM, Bradner JE, Hornick JL, Janicki SM, et al. Activation of SOX2 expression by BRD4-NUT oncogenic fusion drives neoplastic transformation in NUT midline carcinoma. Cancer research. 2014;74(12):3332-43.
4. Kloker LD, Sidiras M, Flaadt T, Brecht IB, Deinzer CKW, Groß T, et al. Clinical management of NUT carcinoma (NC) in Germany: Analysis of survival, therapy response, tumor markers and tumor genome sequencing in 35 adult patients. Lung Cancer. 2024;189:107496.
5. Flaadt T, Wild H, Abele M, Frühwald M, Dirksen U, Classen CF, et al. NUT carcinoma in pediatric patients: Characteristics, therapeutic regimens, and outcomes of 11 cases registered with the German Registry for Rare Pediatric Tumors (STEP). Pediatric Blood & Cancer. 2024;71(3):e30821.
6. Lemelle L, Moya-Plana A, Dumont B, Fresneau B, Laprie A, Claude L, et al. NUT carcinoma in children, adolescents and young adults. Bulletin du Cancer. 2022;109(4):491-504.
7. French CA. Pathogenesis of NUT Midline Carcinoma. Annual Review of Pathology: Mechanisms of Disease. 2012;7(1):247-65.
8. Bauer DE, Mitchell CM, Strait KM, Lathan CS, Stelow EB, Lüer SC, et al. Clinicopathologic Features and Long-term Outcomes of NUT Midline Carcinoma. Clinical Cancer Research. 2012;18(20):5773-9.
9. French CA, Cheng ML, Hanna GJ, DuBois SG, Chau NG, Hann CL, et al. Report of the first international symposium on NUT carcinoma. Clinical Cancer Research. 2022;28(12):2493-505.
10. Lewin J, Soria JC, Stathis A, Delord JP, Peters S, Awada A, et al. Phase Ib Trial With Birabresib, a Small-Molecule Inhibitor of Bromodomain and Extraterminal Proteins, in Patients With Selected Advanced Solid Tumors. J Clin Oncol. 2018;36(30):3007-14.
11. Piha-Paul SA, Hann CL, French CA, Cousin S, Braña I, Cassier PA, et al. Phase 1 study of molibresib (GSK525762), a bromodomain and extra-terminal domain protein inhibitor, in NUT carcinoma and other solid tumors. JNCI Cancer Spectrum. 2020;4(2):pkz093.
12. Shapiro GI, LoRusso P, Dowlati A, T. Do K, Jacobson CA, Vaishampayan U, et al. A Phase 1 study of RO6870810, a novel bromodomain and extra-terminal protein inhibitor, in patients with NUT carcinoma, other solid tumours, or diffuse large B-cell lymphoma. British journal of cancer. 2021;124(4):744-53.
13. French CA, Ramirez CL, Kolmakova J, Hickman TT, Cameron MJ, Thyne ME, et al. BRD–NUT oncoproteins: a family of closely related nuclear proteins that block epithelial differentiation and maintain the growth of carcinoma cells. Oncogene. 2008;27(15):2237-42.
14. Nathan P, Hassel JC, Rutkowski P, Baurain J-F, Butler MO, Schlaak M, et al. Overall Survival Benefit with Tebentafusp in Metastatic Uveal Melanoma. New England Journal of Medicine. 2021;385(13):1196-206.
15. D'Angelo SP, Araujo DM, Abdul Razak AR, Agulnik M, Attia S, Blay J-Y, et al. Afamitresgene autoleucel for advanced synovial sarcoma and myxoid round cell liposarcoma (SPEARHEAD-1): an international, open-label, phase 2 trial. The Lancet. 2024;403(10435):1460-71.
16. D'Angelo SP, Furness AJS, Thistlethwaite F, Burgess MA, Riedel RF, Haanen J, et al. Lete-cel in patients with synovial sarcoma or myxoid/round cell liposarcoma: Planned interim analysis of the pivotal IGNYTE-ESO trial. American Society of Clinical Oncology; 2024.

17. Gazendam AM, Popovic S, Munir S, Parasu N, Wilson D, Ghert M. Synovial Sarcoma: A Clinical Review. Current Oncology. 2021;28(3):1909-20.
18. Knight JC, Renwick PJ, Dal Cin P, Van Den Berghe H, Fletcher CDM. Translocation t(12;16)(q13;p11) in Myxoid Liposarcoma and Round Cell Liposarcoma: Molecular and Cytogenetic Analysis1. Cancer Research. 1995;55(1):24-7.
19. Luo J, Bishop JA, DuBois SG, Hanna GJ, Sholl LM, Stelow EB, et al. Hiding in plain sight: NUT carcinoma is an unrecognized subtype of squamous cell carcinoma of the lungs and head and neck. Nature Reviews Clinical Oncology. 2025.
20. Vensko SP, Olsen K, Bortone D, Smith CC, Chai S, Beckabir W, et al. LENS: Landscape of Effective Neoantigens Software. Bioinformatics. 2023;39(6):btad322.
21. Davar D, Williams A, Lopez J, Olson D, Sato T, Shaw H, et al. 694 Phase 1 safety and efficacy of brenetafusp, a PRAME × CD3 ImmTAC bispecific, in post-checkpoint cutaneous melanoma (CM). Journal for ImmunoTherapy of Cancer. 2024;12(Suppl 2):A796-A.
22. Friedman C, De Burgh Williams A, Lopez JS, Ouali K, Middleton MR, Thistlethwaite F, et al. 750P Phase I safety and efficacy of brenetafusp, a PRAME × CD3 ImmTAC T cell engager, in platinum resistant ovarian cancer (PROC). Annals of Oncology. 2024;35:S569-S70.
23. Beaubier N, Tell R, Lau D, Parsons JR, Bush S, Perera J, et al. Clinical validation of the tempus xT next-generation targeted oncology sequencing assay. Oncotarget. 2019;10(24):2384-96.
24. Michuda J, Breschi A, Kapilivsky J, Manghnani K, McCarter C, Hockenberry AJ, et al. Validation of a Transcriptome-Based Assay for Classifying Cancers of Unknown Primary Origin. Mol Diagn Ther. 2023;27(4):499-511.
25. Finkle JD, Boulos H, Driessen TM, Lo C, Blidner RA, Hafez A, et al. Validation of a liquid biopsy assay with molecular and clinical profiling of circulating tumor DNA. NPJ Precis Oncol. 2021;5(1):63.
26. Huang Y, Durall RT, Luong NM, Hertzler HJ, Huang J, Gokhale PC, et al. EZH2 cooperates with BRD4-NUT to drive NUT carcinoma growth by silencing key tumor suppressor genes. Cancer research. 2023;83(23):3956-73.
27. Kurtenbach S, Sanchez MI, Kuznetsoff J, Rodriguez DA, Weich N, Dollar JJ, et al. PRAME induces genomic instability in uveal melanoma. Oncogene. 2024;43(8):555-65.
28. Spel L, Boelens JJ, van der Steen DM, Blokland NJ, van Noesel MM, Molenaar JJ, et al. Natural killer cells facilitate PRAME-specific T-cell reactivity against neuroblastoma. Oncotarget. 2015;6(34):35770-81.
29. Rosskopf S, Leitner J, Paster W, Morton LT, Hagedoorn RS, Steinberger P, et al. A Jurkat 76 based triple parameter reporter system to evaluate TCR functions and adoptive T cell strategies. Oncotarget. 2018;9(25):17608-19.
30. Pentcheva-Hoang T, Torres D, Rodriguez T, Korngold A, Lu A, Crisostomo J, et al. Inducible MyD88/CD40 (iMC) Enhances Proliferation and Survival of Tumor-Specific TCR-Modified T Cells and Improves Anti-Tumor Efficacy in Myeloma. Blood. 2016;128(22):4550.
31. Scholtalbers J, Boegel S, Bukur T, Byl M, Goerges S, Sorn P, et al. TCLP: an online cancer cell line catalogue integrating HLA type, predicted neo-epitopes, virus and gene expression. Genome Med. 2015;7:118.
32. Wilhelm M, Zolg DP, Graber M, Gessulat S, Schmidt T, Schnatbaum K, et al. Deep learning boosts sensitivity of mass spectrometry-based immunopeptidomics. Nature Communications. 2021;12(1):3346.
33. C. Silva AS, Bouwmeester R, Martens L, Degroeve S. Accurate peptide fragmentation predictions allow data driven approaches to replace and improve upon proteomics search engine scoring functions. Bioinformatics. 2019;35(24):5243-8.
34. Li K, Jain A, Malovannaya A, Wen B, Zhang B. DeepRescore: Leveraging Deep Learning to Improve Peptide Identification in Immunopeptidomics. PROTEOMICS. 2020;20(21-22):1900334.

35. Al-Khadairi G, Decock J. Cancer Testis Antigens and Immunotherapy: Where Do We Stand in the Targeting of PRAME? Cancers. 2019;11(7):984.
36. Doolan P, Clynes M, Kennedy S, Mehta JP, Crown J, O'Driscoll L. Prevalence and prognostic and predictive relevance of PRAME in breast cancer. Breast Cancer Research and Treatment. 2008;109(2):359-65.
37. Epping MT, Hart AAM, Glas AM, Krijgsman O, Bernards R. PRAME expression and clinical outcome of breast cancer. British Journal of Cancer. 2008;99(3):398-403.
38. Takata K, Chong LC, Ennishi D, Aoki T, Li MY, Thakur A, et al. Tumor-associated antigen PRAME exhibits dualistic functions that are targetable in diffuse large B cell lymphoma. The Journal of Clinical Investigation. 2022;132(10).
39. Alekseyenko AA, Walsh EM, Zee BM, Pakozdi T, Hsi P, Lemieux ME, et al. Ectopic protein interactions within BRD4–chromatin complexes drive oncogenic megadomain formation in NUT midline carcinoma. Proceedings of the National Academy of Sciences. 2017;114(21):E4184-E92.
40. Rahman S, Sowa ME, Ottinger M, Smith JA, Shi Y, Harper JW, et al. The Brd4 extraterminal domain confers transcription activation independent of pTEFb by recruiting multiple proteins, including NSD3. Mol Cell Biol. 2011;31(13):2641-52.
41. Fløisand Y, Remberger M, Bigalke I, Josefsen D, Vålerhaugen H, Inderberg EM, et al. WT1 and PRAME RNA-loaded dendritic cell vaccine as maintenance therapy in de novo AML after intensive induction chemotherapy. Leukemia. 2023;37(9):1842-9.
42. Bayat Z, Majidi Z, Taherkhani A, Samie L. Engineering a Novel T-Cell Epitope-Based Vaccine Targeting PRAME in Cancer Immunotherapy. Peptide Science. 2025;117(1):e24393.
43. Chang AY, Dao T, Gejman RS, Jarvis CA, Scott A, Dubrovsky L, et al. A therapeutic T cell receptor mimic antibody targets tumor-associated PRAME peptide/HLA-I antigens. The Journal of Clinical Investigation. 2017;127(7):2705-18.
44. Addis Philip W, Bedke Nicole JOY, Bouard L, Harper S, Liddy N, Mahon T, et al., inventors; IMMUNOCORE LTD, assignee. T CELL RECEPTORS. WO patent WO 2018/234319 A1. 2018 2018/06/19.
45. Froning K, Maguire J, Sereno A, Huang F, Chang S, Weichert K, et al. Computational stabilization of T cell receptors allows pairing with antibodies to form bispecifics. Nature Communications. 2020;11(1):2330.
46. Wu X, Sereno AJ, Huang F, Lewis SM, Lieu RL, Weldon C, et al., editors. Fab-based bispecific antibody formats with robust biophysical properties and biological activity. MAbs; 2015: Taylor & Francis.
47. Kudlacek ST, Metz S, Thiono D, Payne AM, Phan TT, Tian S, et al. Designed, highly expressing, thermostable dengue virus 2 envelope protein dimers elicit quaternary epitope antibodies. Science advances. 2021;7(42):eabg4084.
48. Fagerberg L, Hallström BM, Oksvold P, Kampf C, Djureinovic D, Odeberg J, et al. Analysis of the human tissue-specific expression by genome-wide integration of transcriptomics and antibody-based proteomics. Mol Cell Proteomics. 2014;13(2):397-406.
49. Bruderer R, Bernhardt OM, Gandhi T, Xuan Y, Sondermann J, Schmidt M, et al. Optimization of Experimental Parameters in Data-Independent Mass Spectrometry Significantly Increases Depth and Reproducibility of Results *. Molecular & Cellular Proteomics. 2017;16(12):2296-309.
50. Tognetti M, Sklodowski K, Müller S, Kamber D, Muntel J, Bruderer R, et al. Biomarker Candidates for Tumors Identified from Deep-Profiled Plasma Stem Predominantly from the Low Abundant Area. Journal of Proteome Research. 2022;21(7):1718-35.

Tables:

Fusion	Samples (%)	NC Diagnosis (%)	Primary Site	Samples Per Site (%)
BRD4::NUTM1	59 (36%)	20 (34%)	Unknown primary site	15 (25%)
			Lung	14 (24%)
			Nasal cavity	8 (14%)
			Accessory sinus	4 (7%)
BRD3::NUTM1	18 (11%)	6 (33%)	Lung	7 (39%)
			Unknown primary site	4 (22%)
			Nasal cavity	3 (17%)
			Head, face, or neck	1 (6%)
NSD3::NUTM1	29 (18%)	4 (14%)	Lung	11 (38%)
			Thyroid gland	11 (38%)
			Head, face, or neck	2 (7%)
			Maxillary sinus	2 (7%)
Other	59 (36%)	2 (3%)	Unknown primary site	14 (24%)
			Lung	7 (12%)
			Skin	7 (12%)
			Colon, NOS	4 (7%)

Table 1: Cohort characteristics by *NUTM1* gene fusion partner (N=165).

Figures:

A

	HLA-A		HLA-B		HLA-C	
TC-797	A*02:01	A*02:01	B*18:01	B*07:06	C*05:01	C*07:02
10-15	A*02:01	A*03:01	B*35:01	B*27:02	C*03:03	C*02:02
14169	A*02:01	A*29:02	B*44:02	B*07:02	C*07:02	C*05:01
PER403	A*02:01	A*24:02	B*08:01	B*35:01	C*04:01	C*07:01
JCM1	A*03:01	A*25:01	B*08:01	B*07:02	***	
PDX	A*02:01	A*01:01	B*44:02	B*57:01	C*06:02	C*05:01

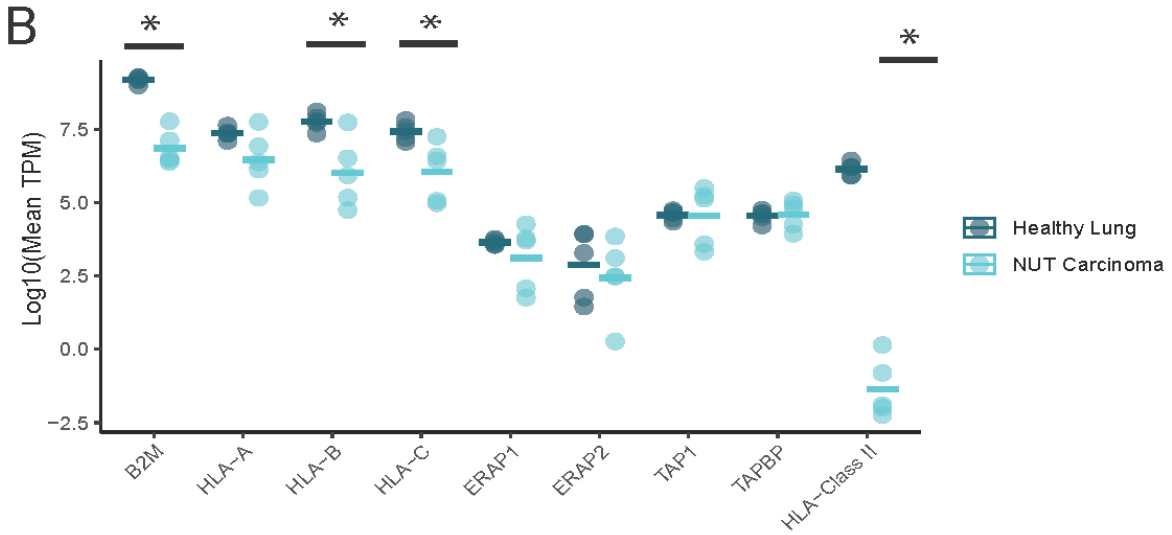

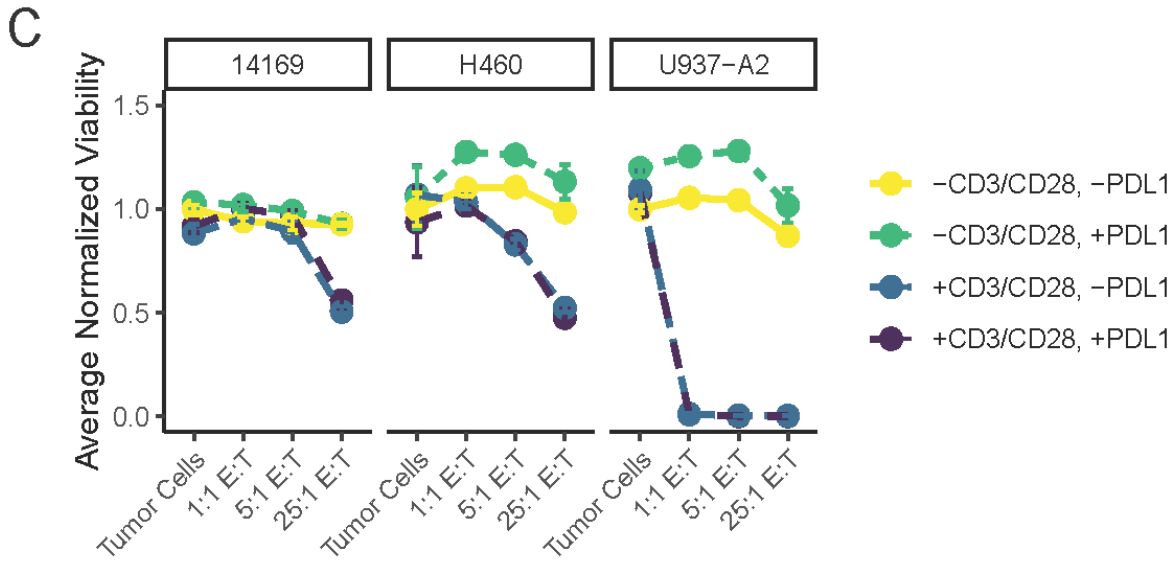

Figure 1 Antigen presentation and allogeneic T-cell killing susceptibility are maintained in NC cell lines (TC-797, 10-15, 14169, PER403, JCM1) and in a PDX. A) HLA haplotypes for these samples. B) RNA Sequencing analysis of HLA Class I and HLA Class II pathway genes in these samples compared to healthy lung. Complete breakdown of HLA Class II genes is given in

Supplemental Figure 1. C) Allogeneic T-cell killing of NC cells are similar to NSCLC cell lines (H460) and less efficient than in a monocytic leukemia line (U937). Additional NC cell lines and NSCLC lines are shown in Supplemental Figure 1 as well. Asterisk (*) indicates $p<0.05$.

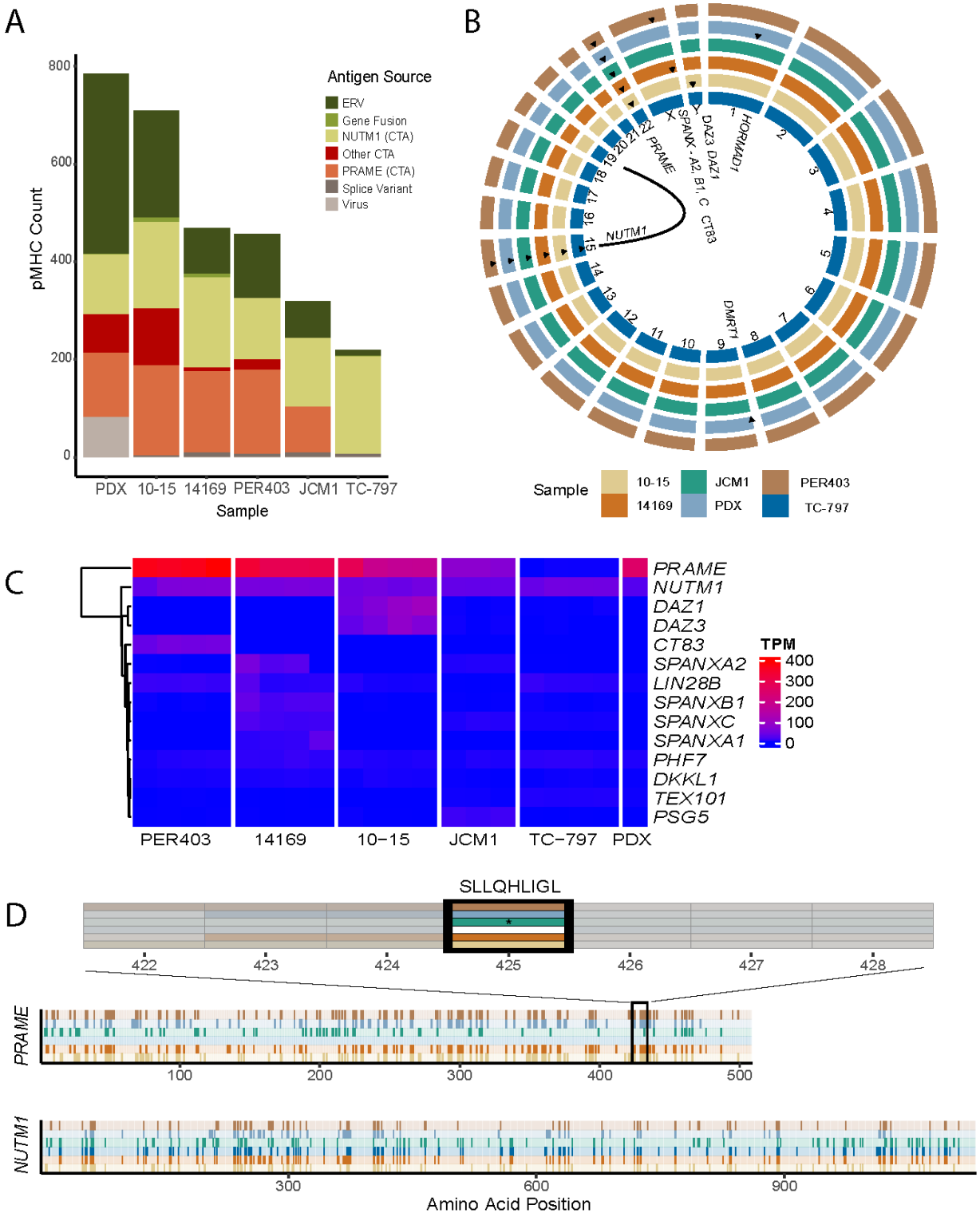

Figure 2 LENS predictions for HLA Class I ligands in NC samples. A) Column plot depicting frequency of different neoantigen types across samples. B) A CIRCOS plot describing the CTAs predicted by LENS. Arrows represent predicted epitopes. Gene names are given within the circle. Arc represents the *BRD4::NUTM1* fusion (note: PDX has a *BRD3::NUTM1* fusion). C) RNA

sequencing heat map of cancer testes genes in these samples. 151 of 165 cancer testes genes were omitted from the heat map as they were transcriptionally silent. D) Predicted epitopes within PRAME and NUTM1 with predicted binding affinities of 500 nM or stronger. Asterisk (*) = predicted binding affinity of 563 nM, slightly weaker than threshold.

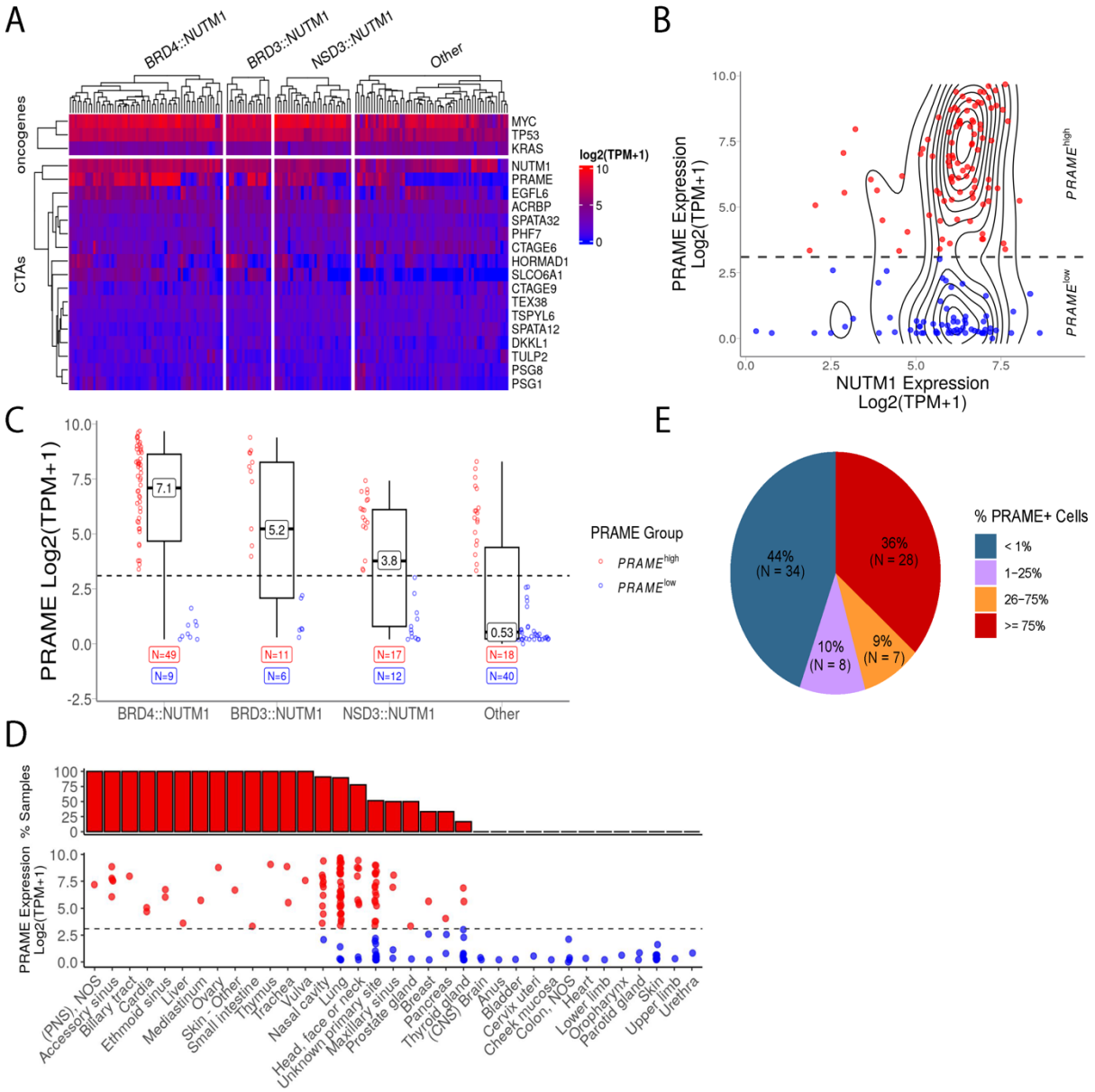

Figure 3 *PRAME* expression in patient samples with *NUTM1* fusion genes. A) Heatmap of most variable CTAs (17 / 157) and relevant oncogenes by *NUTM1* fusion partner. B) *PRAME* and *NUTM1* expression throughout the 165 patient cohort. C) *PRAME* expression by fusion gene. D) *PRAME* expression by anatomic location. E) PRAME staining in a NC tissue microarray.

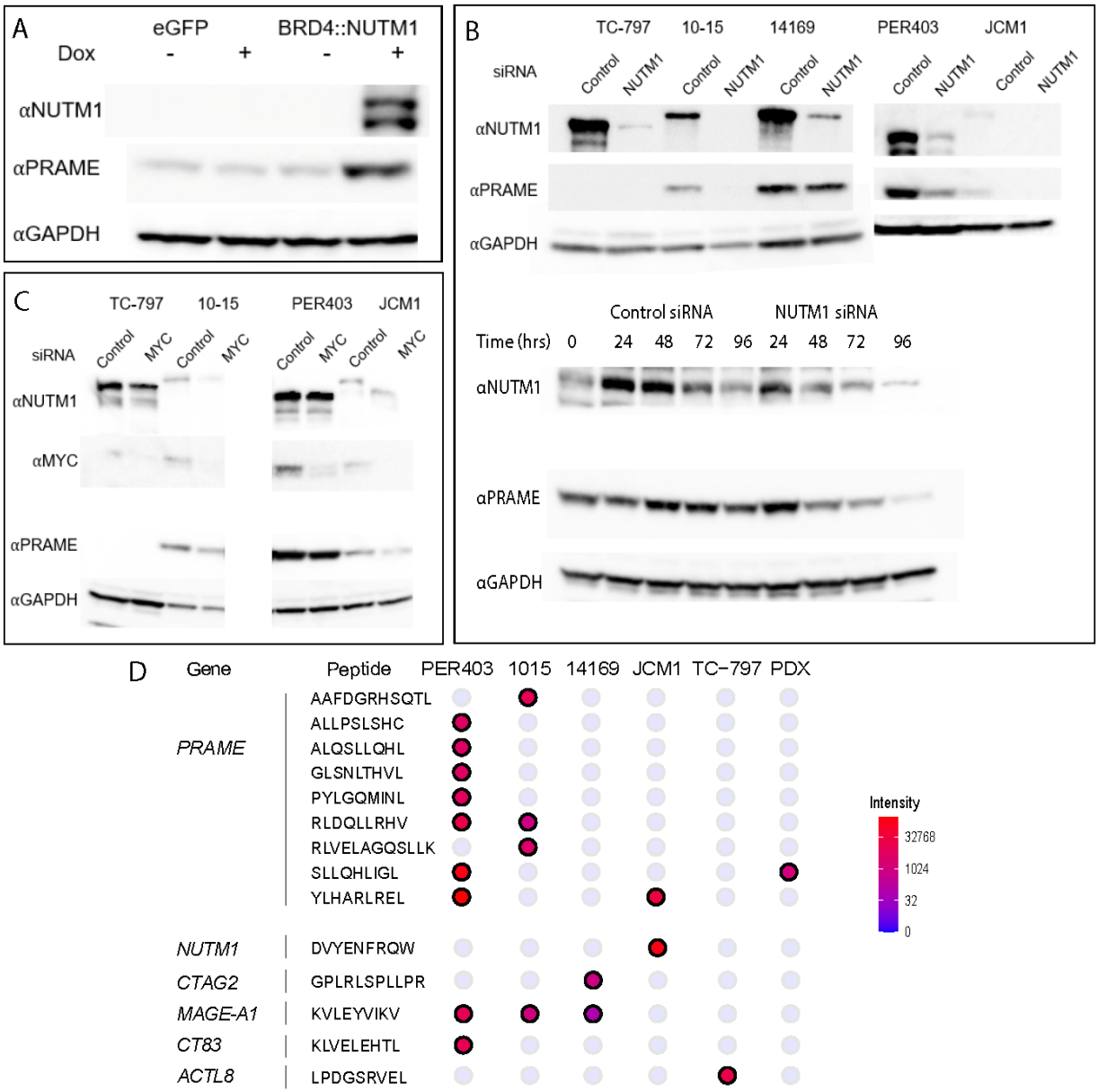

Figure 4 High PRAME levels in NC are maintained by BRD4::NUTM1 and by MYC. A) Immunoblot of HEK 293T cells with a tet-on *BRD4::NUTM1* knock-in showing increased PRAME with BRD4::NUTM1. B) siRNA knockout of *BRD4::NUTM1* using siRNAs targeting *NUTM1* results in lower PRAME levels except in *PRAME*- TC-797 (top). Weak effects in 14169 at 3 days post-transfection prompted a time course (bottom) showing greater PRAME loss at 4 days post-transfection. C) *MYC* siRNA knockout decreases PRAME levels in 10-15, PER403, and JCM1. D) Immunopeptidomics identifies a single NUTM1 epitope in one sample and 9 PRAME epitopes across three samples. Intensity given is a pseudoquantitative metric confounded by differential fragmentation of peptides during mass spectrometry.

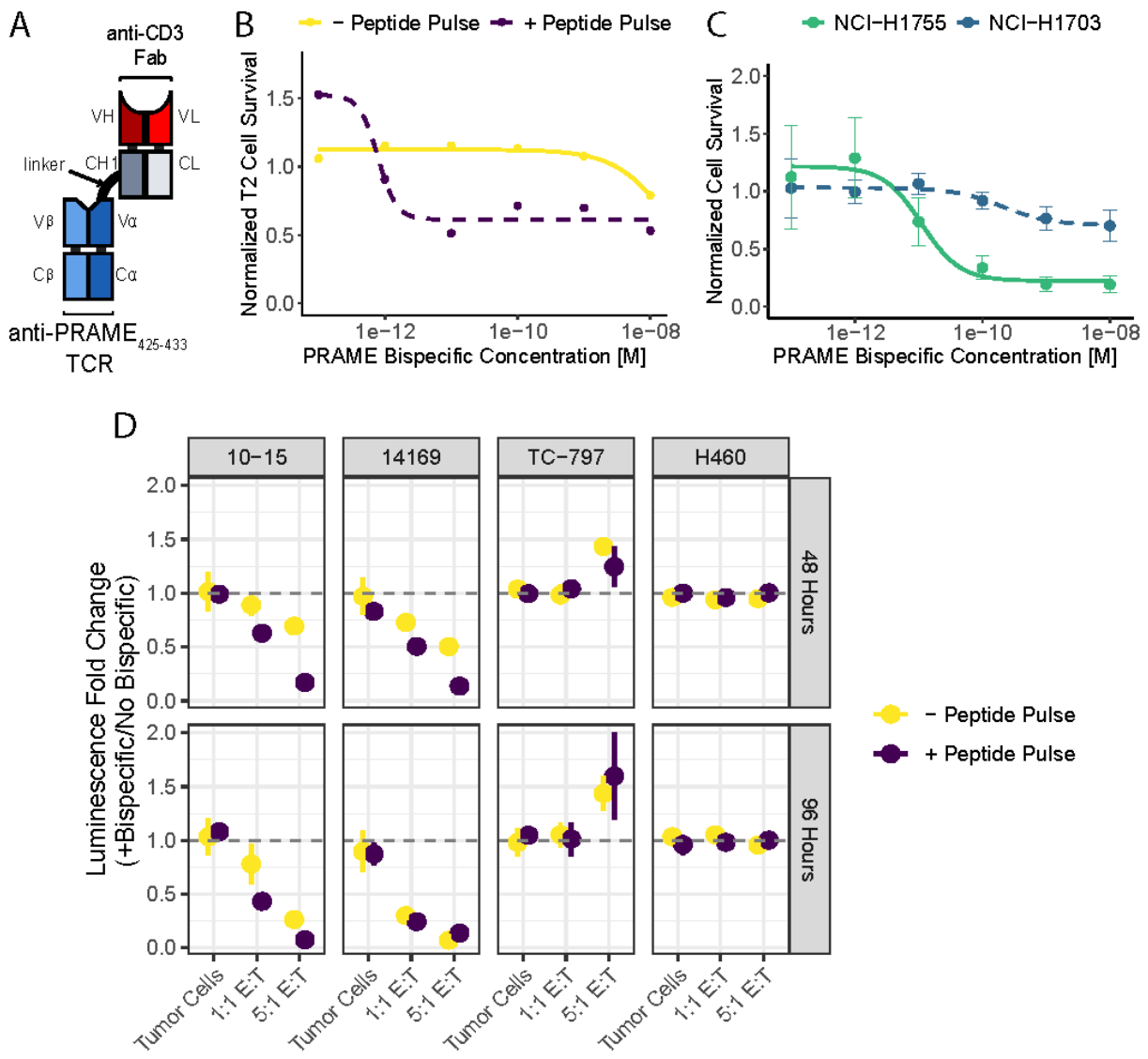

Figure 5 PRAME+ NC cells are susceptible to T-cell killing after incubation with a PRAME TCR x CD3 activator bispecific molecule similar to brenetafusp. A) Diagram showing construction of the bispecific molecule. B) T2 cell cytotoxicity with and without SLLQHLIGL peptide pulse at E:T ratio of 5:1. C) Dose titration of the bispecific molecule in PRAME+ NSCLC lines at E:T ratio of 5:1. D) T-cell cytotoxicity assays with the bispecific in PRAME+ NC cells (10-15, 14169), PRAME- NC cells (TC-797), and in a HLA haplo-incompatible NSCLC line (H460).

Supplementary Figures

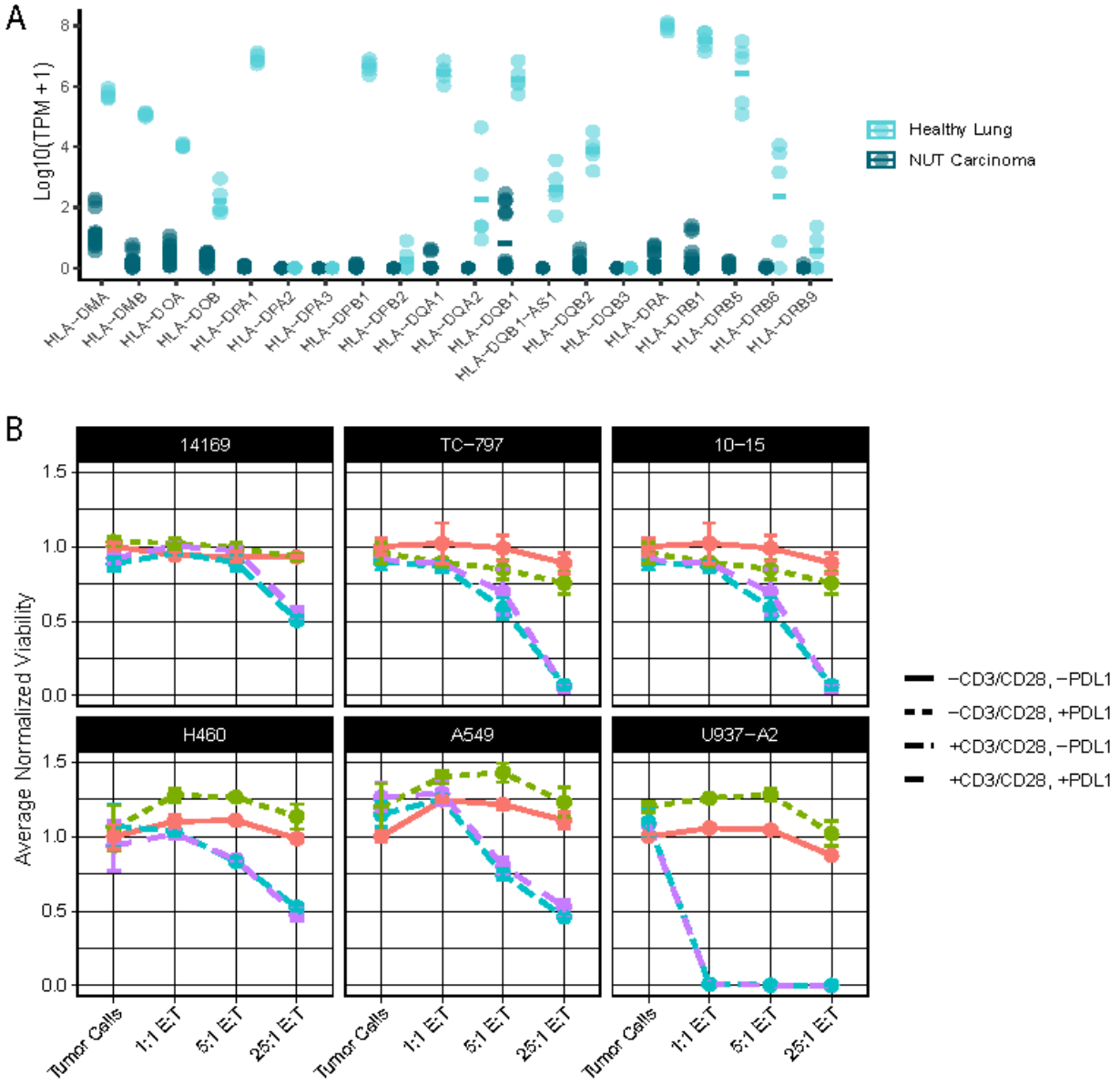

Supplemental Figure 1 MHC Class II genes in NC samples compared to healthy lung (A) and a wider selection of allogeneic T-cell killing assays (B) of NC cells (TC-797, 10-15, 14169), NSCLC cell lines (H460, A549) and leukemia cells (U937).

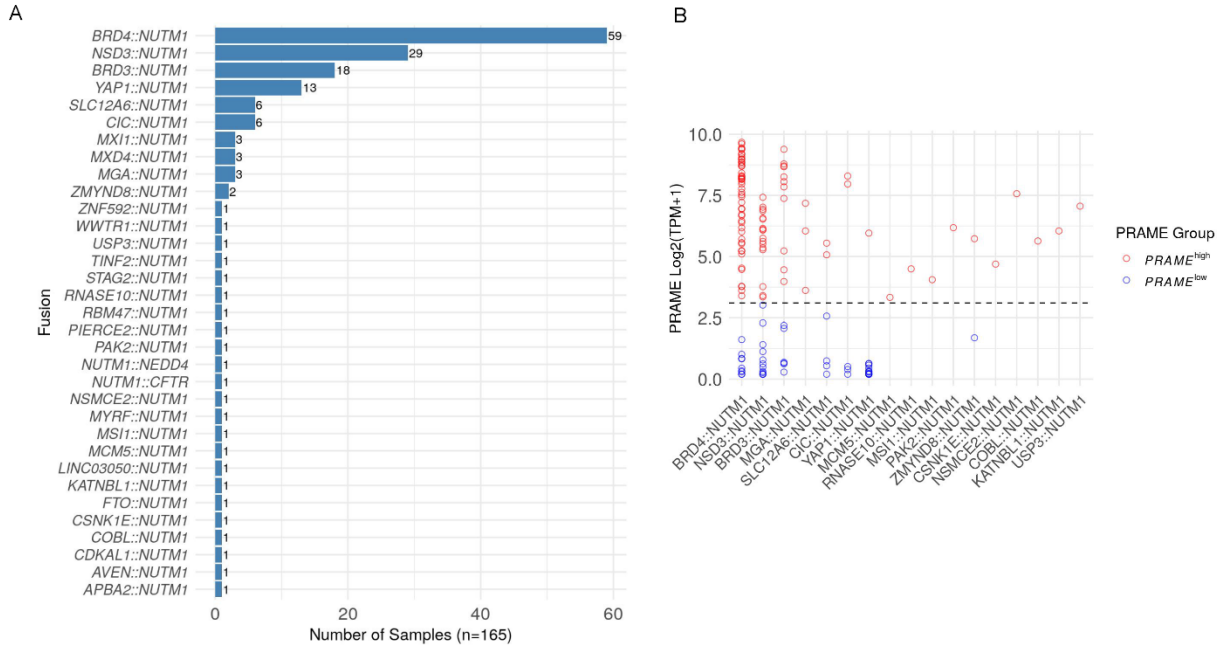

Supplemental Figure 2 Additional data regarding the Tempus clinical cohort. A) Complete list of *NUTM1* gene fusions represented in clinical cohort. B) *PRAME* expression by gene fusion.

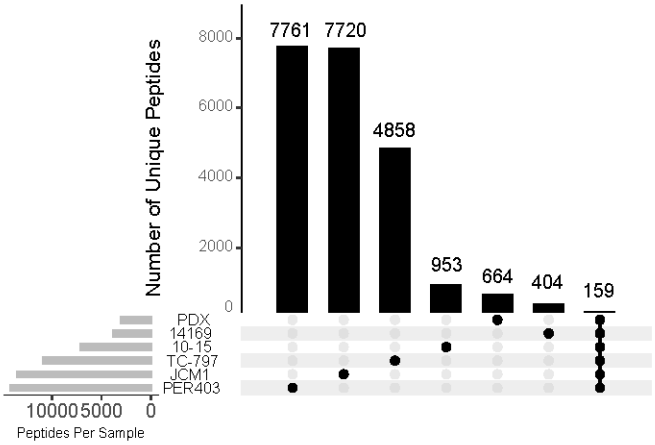

Supplemental Figure 3 Peptide quantitation of the immunopeptidome in five NC cell lines and a PDX.

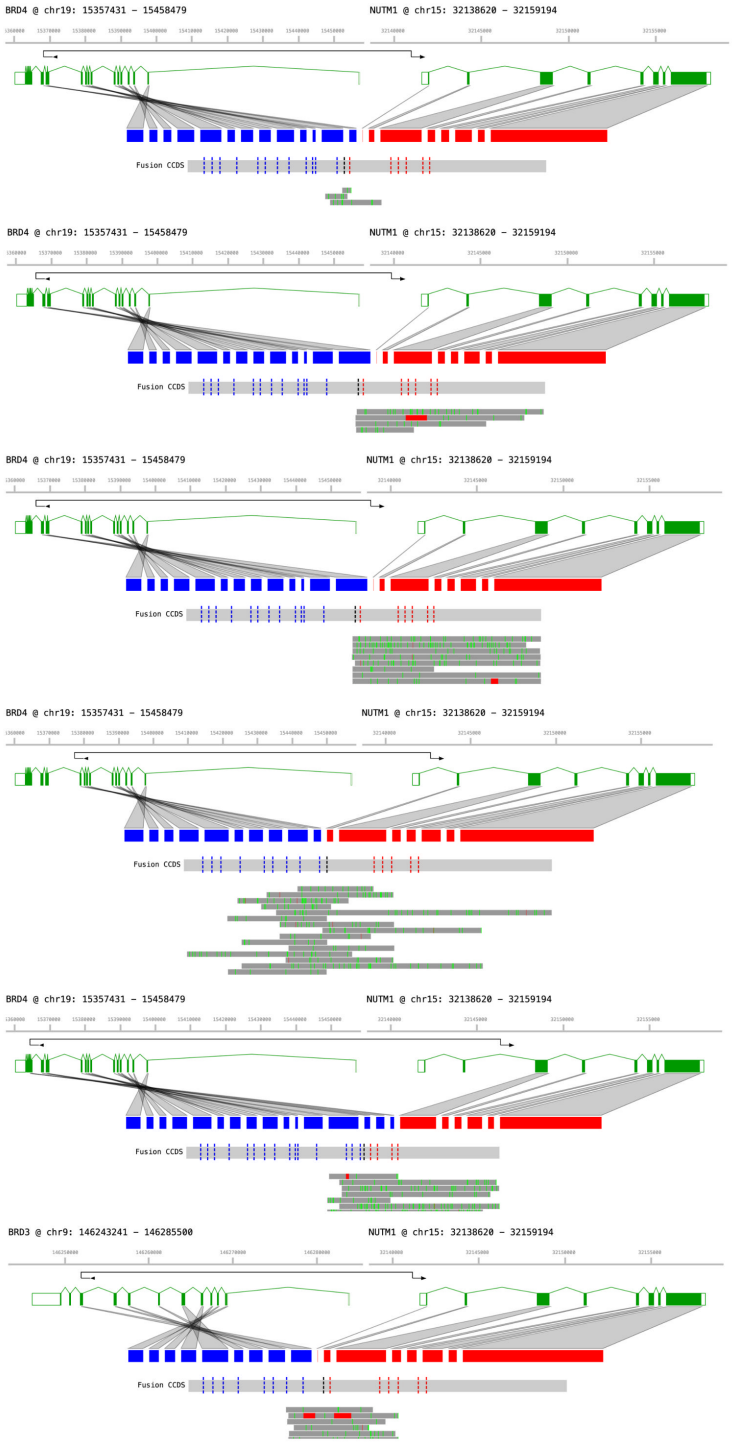

Supplementary Figure 4 Fusion gene characterization of NC cell lines and a PDX using long read RNA sequencing.

Supplementary Methods

Immunoglobulin Target	Vendor, Clone	Dilution
Primary Antibodies		
αNUT	Cell Signaling, Rabbit C52B1	1:1,000
αPRAME	Abcam, Rabbit EPR20330	1:,2000
α-β-Actin	Sigma-Aldrich, A5441	1:10,000
Secondary Antibodies		
αRabbit-HRP	Cell Signaling, Goat #7074S	1:10,000
αMouse-HRP	Cell Signaling, Mouse #7076S	1:10,000

Supplemental Methods Table 1: Western Blotting Antibodies.

siRNA Pool	Sequences
αNUT	
NUTa	AAACUCAGAACUUUAUCCUUA[dT][dT]
NUTa antisense	UAAGGAUAAAGUUCUGAGUUU[dT][dT]
NUTb	AAACUUCUGUUAGUAAAACAC[dT][dT]
NUTb antisense	GUGUUUUACUAACAGAAGUUU[dT][dT]
NUTc	AAUUACCUUUGGAAGGAGCUA[dT][dT]
NUTc antisense	UAGCUCCUUCCAAAGGUAAUU[dT][dT]
NUTd	AAUGGAGAAUCCCAAUGUUGA[dT][dT]
NUTd antisense	UCAACAUUGGGAUUCUCCAUU[dT][dT]
Scrambled controls	
Scrambled a	GAAAUUACUAUCCACUAUCUA[dT][dT]
Scrambled a antisense	UAGAUAGUGGAUAGUAAUUUC[dT][dT]
Scrambled b	GAAUUAACACUACUAUGACUA[dT][dT]
Scrambled b antisense	UAGUCAUAGUAGUGUUAAUUC[dT][dT]
Scrambled c	GAACGAGCUACGGAAUUAUUU[dT][dT]
Scrambled c antisense	AAAUAAUUCCGUAGCUCGUUC[dT][dT]
Scrambled d	GUAAACAACGUGAGACUUAGU[dT][dT]
Scrambled d antisense	ACUAAGUCUCACGUUGUUUAC[dT][dT]

Supplemental Methods Table 2: siRNA sequences.

NUTM1	MAGEA11	SPANXN2	SPATA31D4	TSPY9P	CT47A12
CAGE1	MAGEB1	SPANXN3	SPATA32	TSPY10	CT47B1
PAGE1	MAGEB2	SPANXN4	SPACA1	TSPYL6	CT83
PAGE2	MAGEB3	SPANXN5	SPACA3	MORC1	TEX13A
PAGE3	MAGEB5	ODF1	CATSPERD	TFDP3	TEX19
XAGE1A	MAGEB6B	ODF3	CATSPER4	LUZP4	TEX33
XAGE3	MAGEB16	ODF4	CTAG1A	DKKL1	TEX35
XAGE5	MAGEB18	ROPN1B	CTAG1B	SPO11	TEX37
GAGE2A	MAGEC1	SPAM1	CTAGE1	CRISP2	TEX38
GAGE12H	MAGEC2	SPATA4	CTAGE6	FMR1NB	TEX44
GAGE12J	DAZ1	SPATA12	CTAGE9	TPTE	TEX101
GAGE12E	DAZ3	SPATA16	SSX1	CT45A2	PATE1
GAGE13	DAZL	SPATA19	SSX2	CT45A7	PATE4
MAGEA1	BSPH1	SPATA22	SSX2B	CT47A1	PRSS54
MAGEA2	SPAG11A	SPATA31E1	SSX3	CT47A2	PHF7
MAGEA4	SPANXA1	SPATA31A1	SSX4	CT47A3	SLCO6A1
MAGEA6	SPANXA2	SPATA31A3	TSPY1	CT47A4	TEKT5
MAGEA3	SPANXB1	SPATA31A5	TSPY2	CT47A5	DMRT1
MAGEA9	SPANXC	SPATA31A6	TSPY3	CT47A6	DMRTC2
MAGEA9B	SPANXD	SPATA31A7	TSPY4	CT47A7	DNAJB8
MAGEA10	SPANXN1	SPATA31D3	TSPY8	CT47A11	SAGE1
PSG8	PRM1	PRAMEF18	ACRBP	PRAME	LIPI
PSG11	PRM2	PRAMEF20	TSKS	ACTL8	ADAM2
PSG1	PRM3	CBLL2	CCDC42	SPEM1	PLAC1
PSG3	AKAP4	CPXCR1	ADAD1	THEG	CABS1
CSH2	TNP2	TULP2	RIMBP3	EGFL6	FATE1
PSG5	CGB8	EPPIN	TENT5D	LIN28B	HORMAD1
TRIM64	PSG9				

Supplemental Methods Table 3: Manually curated list of CTAs.

Construct	Amino acid sequence
Primary	EVQLVESGGGLVQPKGSLKLSCAASGFTFNTYAMNWVRQAPGKGLE WVARIRSKYNNYATYYADSVKDRFTISRDDSQSILYLQMNNLKTEDTAM YYCVRHGNFGNSYVSWFAYWGQGTLVTVSAASTKGPSVFPLAPSSKS TSGGTAALGCLVKDYFPEPVTVSWNSGALTSGVHTFPAVLQSSGLYSL SSVVTVPSSSLGTQTYICNVNHKPSNTKVDKKVEPKSCGGGGSGGGG SGGGGSGGGGSGDAKTTQPNSMESNEEEPVHLPCNHSTISGTDYIHW YRQLPSQGPEYVIHGLTSNVNNRMASLAIAEDRKSSTLILHRATLRDAA VYYCILILGHSRLGNYIATFGKGTKLSVIPYIQNPDPAVYQLRDSKSSDK**F** VCLFTDFDSQ**I**NVSQSKDSDVYITDKCVLDMRSMDFKSNSAVAWSNKS DF**T**CANAFNNSIIPEDTFFPSPESSCGGSGGSGGHHHHHHHH
Anti-CD3 auxiliary	QAVVTQESALTTSPGETVTLTCRSSTGAVTTSNYANWVQEKPDHLFTG LIGGTNKRAPGVPARFSGSLIGDKAALTITGAQTEDEAIYFCALWYSNL WVFGGGTKLTVLGQPKAAPSVTLFPPSSEELQANKATLVCLISDFYPGA VTVAWKADSSPVKAGVETTTPSKQSNNKYAASSYLSLTPEQWKSHRS YSCQVTHEGSTVEKTVAPTEC
Anti-PRAME auxiliary	DGGITQSPKYLFRKEGQNVTLSCEQNLNHDAMYWYRQDPGQGLRLIY YSQIMGDEQKGDIAEGYSVSREKKESFPLTVTSAQKNPTAFYLCASSW WTGGASPIRFGPGTRLTVTEDLKNVFPPEVAVFEPS**K**AEIS**R**TQKATLV CLATGFYP**P**HVELSWWVNGKEVH**D**GVCTDPQPLKEQPALNDSRYALS SRLRVSATFWQDPRNHFRCQVQFYGLSENDEWTQDRAKPVTQIVSAE AWGRADC

Supplemental Methods Table 4: Amino acid sequences for primary, anti-CD3 auxiliary, and anti-PRAME auxiliary constructs of PRAME bispecific. CDRs derived from PRAME Vα and Vβ domains are shown in underline. Computationally identified thermostabilizing mutations introduced to PRAME Cα and Cβ domains are shown in bold.